

pubs.acs.org/est Article

# Computational Assessment of the Three-Dimensional Configuration of Dissolved Organic Matter Chromophores and Influence on Absorption Spectra

Elena A. Vialykh, Garrett McKay, and Fernando L. Rosario-Ortiz\*



Cite This: Environ. Sci. Technol. 2020, 54, 15904-15913



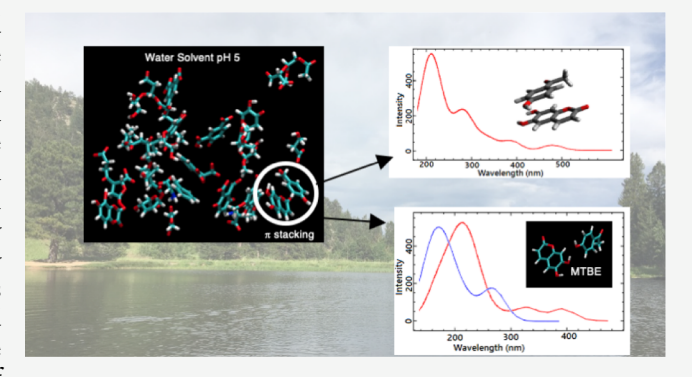
**ACCESS** 

III Metrics & More



S Supporting Information

ABSTRACT: The three-dimensional configuration of dissolved organic matter (DOM) is an important factor in determining the role of DOM in natural and engineered systems, yet there is still considerable uncertainty regarding the formation and potential stability of molecular aggregates within DOM. In this paper, we describe a computational assessment of the three-dimensional configuration of DOM. Specifically, we were interested in evaluating the hypothesis that DOM forms thermodynamically stable molecular aggregates that as a result were potentially shielded from water solvent molecules. Molecular dynamics simulations of DOM model compounds carefully selected based on ultrahigh-resolution mass spectrometry data revealed that, while DOM does indeed form molecular aggregates, the large majority of



molecules (especially, O-atom bearing molecules) are solvent accessible. Additionally, these computations revealed that molecular aggregates are weak and dissociate when placed in organic solvents (tetrahydrofuran, methyl *tert*-butyl ether). Time-dependent density functional theory calculations demonstrated long-wavelength absorbance for both model DOM chromophores and their molecular aggregates. This study has important implications for determining the origin of DOM optical properties and for enhancing our collective understanding of DOM three-dimensional structures.

# ■ INTRODUCTION

Chromophoric dissolved organic matter (CDOM) is the lightabsorbing fraction of DOM and is the main absorber of sunlight in aquatic systems. <sup>1-4</sup> Although representing only a fraction of the overall DOM pool, CDOM optical measurements (absorbance and fluorescence) are widely utilized to infer the DOM structure and chemical composition in natural and engineered systems. 5-8 CDOM also represents the photochemically active fraction of DOM, resulting in the formation of different reactive intermediates, which influence the degradation of dissolved species in surface waters. 9-11 One of the most common methods to characterize DOM is via the measurement of its absorbance spectra. A common feature of CDOM absorbance is the exponential decrease in absorbance with increasing wavelength; <sup>3,12</sup> very rarely, specific peaks are observed, and if so, they have been observed in the UV region of the spectrum.<sup>13</sup> This well-known shape of the absorbance spectra is the basis for the development of numerous optical indices (e.g., spectral slope, E2/E3, and so forth) that are used to characterize DOM and derive useful assessments regarding its physicochemical properties. 14,15

Although the absorbance of DOM is widely used to infer its behavior, we still do not have a clear understanding of the fundamental model that explains the observed exponential decay, or its photophysical properties (this statement also extends to the understanding of the fluorescence of DOM, although our focus herein is on absorbance). Two models have been proposed to describe the photophysical properties of CDOM. <sup>12,13,16–18</sup> The superposition model indicates that the observed absorbance is the result of noninteracting chromophores, where the sum of absorbance spectra of all components results in the universally observed exponential decay. This model rests on several assumptions, including that there are groups within DOM that can absorb in the visible range (wavelengths > 350 nm), which is not the case for many organic chromophores, especially those that have been wellcharacterized in CDOM (e.g., phenols, quinones, and so forth). Alternatively, an electronic interaction model has been proposed in which electron-rich donors (D) associate with electron-poor acceptors (A) to form complexes capable of undergoing charge-transfer (CT) excitation (D + A  $\rightleftharpoons$  DA +

Received: August 31, 2020 Revised: November 12, 2020 Accepted: November 18, 2020 Published: December 3, 2020





 $h\nu \rightarrow [D^+A^-]^*$ ). 12,19-21 This model states that CDOM optical properties include contributions from individual chromophores in addition to DA complexes. There are clear implications of these two models for other aspects of DOM chemistry, including the photochemical reactivity and the use of optical metrics to infer DOM properties, and the authors refer the reader to other publications for a more in-depth discussion of these other issues. 13

Recently, there has been a discussion in the literature centered around the plausibility of the CT model to act as a major photophysical model for DOM. McKay, Korak, and coworkers 16 presented evidence on the lack of impact that changes in solvent polarity, temperature, and viscosity had on the optical properties. The results were interpreted as evidence that CT is not the main photophysical mechanism explaining the optical properties of DOM, although the data cannot categorically reject the presence of CT on a smaller scale. This interpretation rests on the known behavior of CT states as a function of changing chemical environments. For example, no significant differences were observed in the absorbance spectra when different DOM isolates were dissolved in solvents of varying polarities. In their rebuttal of work by McKay, Korak et al., 16 Blough and Del Vecchio 17 proposed that CT states were indeed a dominant pathway, and that the lack of changes in the optical properties due to solvent, temperature, and viscosity, was due to the solvent inaccessibility of components associated with the CT states. This hypothesis infers that most CT active groups, which would represent groups with high electronwithdrawing (e.g., quinones, aromatic ketones/aldehydes, so forth) and electron-donating (e.g., phenols, hydroxy benzoic acids, and so forth) abilities, would be inaccessible to the aqueous phase. Blough and Del Vecchio 17,18 support this hypothesis based on the evidenced microheterogeneous distribution of singlet oxygen production from CDOM<sup>22</sup> and the slow chemical/electrochemical reduction of DOM compared to that of model electron acceptors.<sup>23</sup>

Given the complexities in the study of DOM, it is challenging to gain an in-depth mechanistic understanding of the system without reducing this complexity. This has been done in past studies by focusing on the use of model compounds to study the optical and photochemical properties of DOM.<sup>24–26</sup> Conversely, in the case of evaluating competing models for CDOM photophysics, most work has been based on chemical (e.g., oxidation/reduction, protonation/deprotonation) and physical (e.g., molecular weight fractionation) modifications, and subsequent assessment of these treatment's impacts on optical and photochemical properties. 18,25,27-2 However, given the DOM's complexity, it is difficult to design an experiment that will categorically accept or reject the hypothesis that CT sites are inaccessible to the solvent. In such applications where experimental verification would be difficult to obtain, the use of computational models can provide an

Over the past 30 years, there have been numerous studies examining the complexity of DOM using computational methods.  $^{30-34}$  In this work, we employed the latest perception of DOM as labile supramolecular assemblies<sup>35</sup> and used a computational modeling technique that allowed us to simulate noncovalent interactions, which include H-bonding, hydrophilic/hydrophobic interactions,  $\pi$ -stacking, as well as covalent bond formation and breaking.3

We used this computational modeling framework to assess the effect that the three-dimensional composition of DOM

would have on the solvent accessibility of known chromophores within DOM. We were interested specifically in testing the hypothesis of Blough and Del Vecchio<sup>12</sup> that the majority of CDOM chromophores are inaccessible to solvent molecules. To accomplish this, we developed a series of structural models of DOM based on data from high-resolution mass spectrometry. The models were then examined computationally by equilibrating in three different solvents, and the solventaccessible surface area (SASA) was estimated. Finally, the absorbance spectra for individual noninteracting components and their observed aggregates were calculated. The large majority of chromophores within our models were solvent accessible, suggesting that this may also be the case for DOM in the environment. Importantly, we show that  $\pi$ -stacked structures within DOM do contribute to visible absorbance, but that this contribution represents a small portion of the overall absorbance spectrum.

### MATERIALS AND METHODS

Generation of DOM Models. In this work, five models representing Suwannee River fulvic acid (SRFA) were developed. The models were created on the basis of SRFA chemical characteristics<sup>37</sup> using principles proposed by Vialykh et al.<sup>38,39</sup> The following algorithm of fragment selection from FTICR-MS data was implemented: (1) three chromophores identified in DOM were selected; (2) three molecules with the highest intensity in SRFA FTICR-MS data<sup>42</sup> were added to the previous molecules; (3) average parameters (see Screening Criteria below) for selected molecules were calculated; and (4) 2 to 15 molecules from FTICR-MS data were added to previously selected ones such that the average chemical characteristics described in Screening Criteria of each model were in agreement with experimental data for SRFA, and the number of atoms ranged between 450 and 500. Structural formula for fragments with molecular sizes between 100 and 450 Da was selected from structures presented in PubChem<sup>43</sup> for a particular empirical formula. The structures for fragments with molecular weight above 450 Da were obtained from Leenher et al.<sup>37</sup> The composition of the models is presented in the Supporting Information The primary difference between the five models was in the size of selected molecules. Thus, model #1 was composed of molecules with a molecular weight range 118-760 Da, models #2-5 contained fragments with a molecular weight in the range 118-258, 152-486, 146-760, and 196-540 Da, respectively.

The developed SRFA models were equilibrated in the following three solvents: water, methyl tert-butyl ether (MTBE), and tetrahydrofuran (THF). These solvents were chosen based on their differences in octanol/water partition coefficient and dielectric constants and were chosen to simulate the effect of the change in the solvent polarity on the equilibrium three-dimensional configurations of the created models. Based on the work published by Vialykh et al., 38,39 the concentration of organic matter in the developed models was chosen as ~20% (mol/g of organic matter per mol/g of solvent), which was necessary to achieve reasonable computational timeframes and at the same time allow investigation of solvent effect on the 3D configuration of DOM and its functional behavior in different solvents. For the different solvents employed, it was thus necessary to add 1000 water molecules, 250 molecules of THF, or 205 molecules of MTBE. The organic matter concentration should not affect the interpretation of our results because this comparatively high

concentration will actually favor intermolecular interactions. For comparison, the model of DOM #1 was simulated with the concentration of organic matter  $\sim 7\%$  at pH 5. Thus, 3000 water molecules were added, whereas 1000 water molecules were added to achieve a concentration of  $\sim\!20\%$ . In every solvent, the organic mixtures were modeled with deprotonated carboxylic groups and protonated hydroxyl groups, which allows the pH of the systems to be considered  $\sim\!5-6.^{44}$  To keep the overall charge of the models equal to zero and compensate the negative charge of deprotonated groups, Na<sup>+</sup> ions were added. However, when the calculations were performed in an aqueous environment, additional modeling with both deprotonated carboxylic and hydroxyl groups was performed, thus allowing one to consider the pH of the system  $\sim 10.$ 

Screening Criteria. One of the goals of this study was to evaluate the propensity of DOM to form stable and/or static hydrophobic cores, which would exclude water as a solvent, and influence the observed physicochemical properties. To make this assessment computationally, it is important to carefully select the initial molecular structures to include in the model, which could significantly affect the functional behavior of the system. For the fragments with a molecular weight below 350 Da, it was possible to identify specific chemical structures for the unique molecular formulas identified in SRFA FTICR-MS data. 41 However, when the molecular size increased, the number of possible structural isomers for the given formula increased significantly. To limit the number of possible structures, the following characteristics of SRFA were used as screening criteria: carbon distribution by the type of functional group (aliphatic, heteroaliphatic, aromatic, phenols, carboxyl, esters, and ketones), hydrogen distribution (exchangeable hydrogen, including carboxyl, phenol, and alcohol, and nonexchangeable, including isolated aliphatic and aromatic), oxygen distribution (carboxyl, ester, ketone, phenol, alcohol, acetal and ketal, ether), and carbohydrate ratio<sup>37</sup> (Text S1, Supporting Information). This manual screening process of the possible structures identified by PubChem ruled out the selection of hydrophobic compounds composed of a large number of unsubstituted rings (e.g., naphthalene), primarily because the aromaticity criteria were exceeded.

Exclusion of the structures with unsubstituted aromatic rings is also in agreement with the aqueous solubility requirement of molecular components observed in nature. Calculation of log D, where D is the distribution coefficient for ionizable compounds, for individual molecules with MarvinSketch<sup>45</sup> showed that most selected fragments have a log D below zero at pH 5 (Figure S1 and Table S1, Supporting Information). In comparison, molecules like benzene, naphthalene, or toluene have a log D above zero (1.97, 2.96, and 2.49, respectively). Based on this analysis, we conclude that the presence of a hydrophobic core would severely limit the inherent solubility of DOM. This is in stark contrast to the well-known high solubility of DOM. Indeed, vapor pressure osmometry studies by Aiken and Malcolm<sup>46</sup> revealed exceedingly high amounts of SRFA solubilized in THF (>1 mg/mL). In our computational assessment, as we expect most of the fragments to be water soluble (DOM is indeed highly water soluble), we hypothesize that the number of fragments able to form the hydrophobic core will be limited.

**Molecular Dynamics Simulations.** In total, 21 systems were generated (five models, in three solvents, with additional six simulations in water). The systems were packed using

Packmol software<sup>47</sup> with periodic boundary conditions. The ReaxFF protein force field was used to perform the molecular dynamics (MD) simulations and energy minimizations of the models. The ReaxFF force field was chosen, because in work done by Vialykh et al., 38 it was shown that possible covalent bond formation and breaking could occur in humic materials, such as resonance-induced intramolecular keto-enol proton-transfer interaction, which could be important in further evaluation of UV-absorbance spectra of DOM. Detailed description of the ReaxFF force field is provided in the Supporting Information (Text S2). Parallel simulations were run with the classical MD package LAMMPS.50 The energy of each system was initially minimized using the ReaxFF force field. Geometry optimizations were deemed to have converged when the root mean square of forces fell below 0.1 kcal mol<sup>-1</sup> A<sup>-1</sup>. NVT-ensemble (constant number of particles, volume, and temperature) simulations were run for the first 0.25 ns (with temperature 300 K), followed by NPT-ensemble (constant number of particles, pressure, and temperature) simulations (P = 1 atm and T = 300 K) that were run until the size of the periodic box stabilized (variation in one dimension less than 1%). The size of the box varied between 29 and 34 Å. Furthermore, NVTensemble simulations were run for 0.15 ns with the temperature increase from 300 to 600 K and the size of the periodic box obtained from the previous step. Coordinates from the last step in NVT-ensemble simulations were used as initial coordinates for replica exchange MD (REMD) simulations at desired temperatures. Overall, 36 replicas were used for REMD simulations with the temperature spaced in a geometrical distribution in a range 300-550 K. Each replica was simulated for 3 ns with a total simulation time of 108 ns. The exchange of temperature was attempted every 2000 steps. In order to maintain the desired exchange ratio, it was evaluated every 0.05 ns, followed by temperature adjustments. All the calculations utilized an MD time-step of 0.25 fs. During simulations, the system temperature and pressure were controlled by the Nóse-Hoover thermostat and barostat with 0.1 and 1.0 ps damping constants, respectively.

Combined data for all replicas from REMD were analyzed using a weighted histogram analysis method (WHAM) to obtain the potential of mean force (PMF) at 300 K as a function of radius of gyration  $(R_G)$  of DOM models. RMF is referred to as the free energy surface along the chosen coordinate. R<sub>C</sub> is defined as the root-mean-square average of the distance of all scattering atoms from the center of mass of the molecule<sup>51</sup> and was calculated for the whole DOM aggregate.  $R_G$  could be used as an indicator of DOM aggregate compactness. The VMD<sup>52</sup> tools together with in-built commands were used for the correct determination of R<sub>G</sub> that allows to take in account periodic boundary conditions. From the last 0.1 ns of MD simulations, frames with coordinates that correspond to  $R_G$  at the lowest relative free energy were selected for further analysis. The following parameters of DOM models were determined: SASA, hydrophobic and hydrophilic surface areas (HbSA and HpSA), number of hydrogen bonds, and formation of  $\pi$ -stacking. Analysis of SASA and hydrogen bonding was performed with UCSF CHIMERA<sup>53</sup> software. To calculate HbSA and HpSA, SCHRODINGER<sup>54</sup> software was used.

**Absorbance Spectra Calculations.** The ORCA 4.0.1 package<sup>55</sup> was used to carry out geometry optimizations and spectral calculations for individual molecules,  $\pi$ -stacking

clusters, and molecular aggregates. Geometry optimizations were performed using the B3LYP functional with the def2-TZVP basis set in water solvent with an SMD solvation model. Tight self-consistent field convergence criteria were set without symmetry constraints. The RIJCOSX approximation was used with the auxiliary basis def2/J to accelerate the calculations without notable loss of accuracy.

The TD-DFT and sTD-DFT calculations were performed using the B3LYP or BP86 functional on the DFT-optimized structures with def2-TZVP or aug-cc-pVDZ basis sets. The RIJCOSX approximation was employed to speed up the calculations. The SMD solvation model was used to conduct the calculations in water solvent. The calculation of the charge transfer in the excited states has been performed by the TheoDORE program package. 56,57

# RESULTS AND DISCUSSION

Molecular Dynamics Simulations. In this work, REMD simulations were chosen over the conventional MD simulations, as the improved sampling provided by the REMD technique allows us to explore the configuration space of our DOM models in three different solvents that could be difficult to explore at low temperatures. To ensure convergence of the simulations, we evaluated the temperature evolution of individual replicas during the simulations. Figure S2, Supporting Information, presents the time series of replica sampling at a temperature of 300 K for model #1 in water solvent at pH 5. One of the challenges of MD simulations is increasing the sampling of low-energy structures at the lowest temperature, which tend to be kinetically trapped at lower temperatures. Higher temperatures allow these high activation energy interactions to be overcome and speed up the other interactions. Therefore, the observed free random walk in the temperature space in REMD simulations confirmed a correct evolving of the simulations and ensures that the system was not trapped in one of the local minima. The other 35 replicas similarly explore the full spectrum of temperatures, moving in the course of the simulation from the lowest to the highest temperature and back, leading in this way to increased sampling of low-energy structures at the lowest temperature. A similar temperature evolution of replicas was observed in REMD simulations for other models with different solvents. The acceptance ratio between two temperatures is determined from the overlap of their respective potential energy distributions. The desired range for the exchange acceptance ratio should be greater than 0.158 and in-between 0.20 and 0.30. 59,60 To maintain the ratio in the desired range, the initial temperatures for replicas were chosen according to the relation  $T_i = T_0 \cdot \exp(i \cdot c)$ , 58 where  $T_0 = 300$  K and c is varied to give the desired ratio. As shown in Figure S3, Supporting Information, the probability distributions of potential energy (model#1, water solvent, pH 5) have the desired behavior with enough overlap between each adjacent temperature pairs to allow exchange to occur. In effect, this approach allows adequate sampling of the space of all system's possible confirmations to ensure that the systems were not trapped in local minima. We can thus be confident that the systems reached the global minimum that correspond to system's conformation at the equilibrium point.

Energy Minima in MD Simulations. In comparison with the conventional MD simulations, where the time average over the entire ensemble gives values that could be compared with the experimental results, in REMD simulations based on

statistical analysis PMF could be generated. PMF is a tool that allows examining the free energy variation as a function of one or more specific reaction coordinate(s) for a given system. Implementation of the PMF in the simulations can help overcome the difficulties in sampling specific regions on the energy landscape and provide useful insights to understand the reaction mechanism. As the calculation of PMF usually requires many, possibly parallelizable, short simulations instead of a few extremely long simulations, these simulations, therefore, are fairly manageable.<sup>61</sup>

Trajectories from REMD simulations were further analyzed by WHAM<sup>62–64</sup> to obtain the PMF as a function of  $R_G$ . Based on the understanding of humic substances as supramolecular aggregates of smaller components, we chose  $R_{\rm G}$  as a criterion to evaluate the 3D conformation of the aggregates of our DOM models in different solvents. R<sub>G</sub> was calculated for the whole DOM aggregates. Free energy minima from PMF allows determining the most stable confirmations of the DOM aggregates at equilibrium. Thus, in this work, we evaluate the characteristics of the most probable/stable confirmations of the aggregates at equilibrium. The shape of PMF (Figure 1)

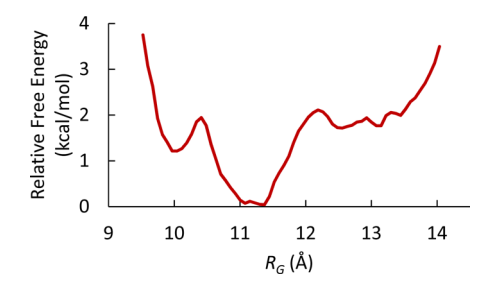


Figure 1. Relative free energy change as a function of radius of gyration (R<sub>G</sub>) calculated by WHAM for model #1 at pH 5 in water solvent.

shows many local minima, but the two lowest are in the region of 11.0 to 11.4 Å. The energy difference between these two minima, with  $R_G$  equal to 11.08 Å and 11.39 Å, is only 0.02 kcal/mol. Moreover, for R<sub>G</sub> between 9.6 and 13.5 Å, the energy barrier between different minima was less than 2.5 kcal/mol. These energy barriers are insignificant in comparison with the energy of a H-bond of  $\sim 1-3$  kcal/mol and the thermal energy available at 300 K ( $\sim$ 0.6 kcal/mol). Thus, for DOM, there will not be a highly preferred assembly under environmental conditions and, more importantly, there will be several different assemblies present at thermal equilibrium with concentrations of the same order of magnitude as the optimum assembly at any point in time. Similarly, in other works, 65attempts to find the global minima of humic acids' molecular fragments or aggregates demonstrated the formation of flexible networks with voids, with several assemblies with very close energies. This conclusion has implications for how we think about DOM assemblies, both in terms of their stability and also the observed physicochemical properties of the system. Figure 2 shows the 3D confirmations for model #1 at pH 5 in water solvent and THF, after MD simulations (and the corresponding videos are available as part of the Supporting

Quantitative Characterization of Computational **Models.** The last 0.1 ns of the replica at 300 K of REMD simulations was further analyzed. The snapshots of coordinates that correspond to the  $R_G$  at a relative free energy equal to zero

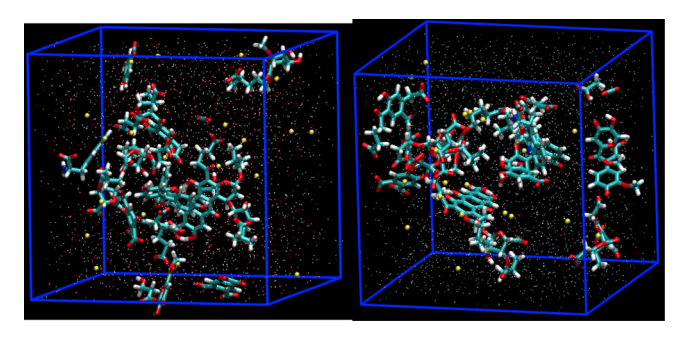
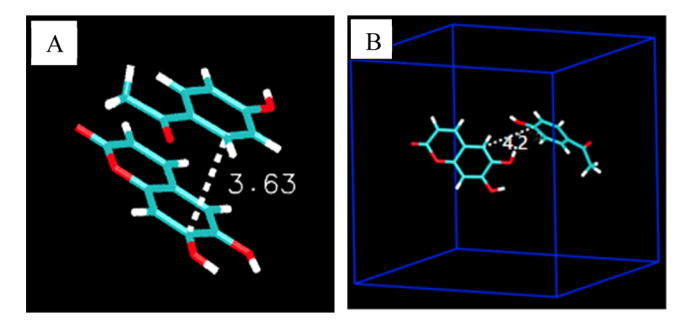


Figure 2. Snapshot of 3D configurations of model #1 at pH 5 in water (left) and THF (right) solvent at equilibrium. Atoms are colored as follows: carbon—blue, oxygen—red, hydrogen—white, nitrogen—dark blue, and Na—yellow. The dots represent the solvent.

were selected; for example, model #1 at pH 5 solvated with water had an  $R_{\rm G}$  equal to 11.39 Å (Figure 1). SASA, HbSA, and HpSA were analyzed (Table 1). All the five DOM models solvated in water at pH 5 with concentration  $\sim$  20% were the most compact of those analyzed, having the smallest SASA and HpSA. The lowest number of H-bonds was observed in models with water solvent at pH 10 because most of the functional groups were deprotonated. These pH 10 models were also less compact, which can also be rationalized by their deprotonation. Simulations for model #1 at pH 5 ( $\sim$ 7% DOM concentration) resulted in an increase of  $R_{\rm G}$  to 16.91 Å. The 3D configurations in less polar solvents, MTBE and THF, were not as compact as in water solution with the same concentration as from the higher  $R_{\rm G}$  observed for SRFA dissolved in these two organic solvents.

Regarding specific structural configurations in water, we observed that two to four molecular fragments (out of 8-23 molecules) were involved in the formation of  $\pi$ -stacking



**Figure 3.** (A) Configuration of the  $\pi$ -stacking cluster formed between esculetin and hydroxyacetophenone in model #3 with water solvent at pH 5. The distance between aromatic ring centers is 3.6 Å. (B) 3D conformation of the molecular fragments after REMD simulation in THF solvent. The distances between the nearest carbon atoms are 4.2 and 7.0 Å between the centers of the aromatic rings.

clusters in every model (Figure 3a). In the model with 3000 water molecules (~7% DOM concentration), although the aggregation occurred to a lower extent, the formation of  $\pi$ stacking clusters was still observed. Beyond the hydrophobic/ hydrophilic, van der Waals, electrostatic, and the abovediscussed  $\pi$ -stacking interactions, proton transfer between organic matter and water molecules occurred in each model with water solvent. In nonpolar solvents,  $\pi$ -stacking clusters did not form. To verify this result, additional tests were run in which  $\pi$ -stacking clusters that formed in water were placed in nonpolar solvents (10% organic matter concentration) and REMD simulations were performed. For example, the initial distance between the centers of the molecules (esculetin and hydroxyacetophenone) in the  $\pi$ -stacked cluster formed in water was  $3.63 \pm 0.2$  Å. Upon addition to THF (Figure 3b), this distance increased up to  $7.00 \pm 0.3$  Å. Similar behavior was

Table 1. Quantitative Characteristics Derived from Molecular Dynamics Simulations, including  $R_G$ , SASA, HbSA, HpSA, and Number of H-Bonds<sup>a</sup>

model #	Solvent	$R_{\rm G}$ (Å)	SASA (Å <sup>2</sup> )	HbSA (Ų)	HpSA (Ų)	number of H-bonds	change in SASA <sup>b</sup> , %
1	water pH 5	11.39 (0.11)	4293 (112)	173 (21)	4208 (65)	5.0 (0.4)	32.1
	water pH 10	12.74 (0.13)	5501 (134)	123 (19)	5465 (97)	2.3 (0.3)	12.9
	MTBE	14.10 (0.12)	5701 (163)	335 (47)	4884 (30)	5.5 (0.5)	9.9
	THF	13.34 (0.13)	5567 (160)	381 (30)	4652 (21)	5.7 (0.6)	12.0
	3000WM pH 5	16.91 (0.51)	5975 (210)	142 (22)	5059 (87)	4.5 (0.4)	5.5
2	water pH 5	13.44 (0.38)	5431 (229)	220 (62)	4156 (453)	3.5 (0.6)	21.3
	water pH 10	13.79 (0.22)	5956 (212)	83 (51)	5260 (327)	2.0 (0.6)	13.6
	MTBE	14.09 (0.21)	5962 (202)	386 (53)	4701 (223)	7.3 (0.4)	13.5
	THF	14.53 (0.61)	6219 (170)	469 (67)	4949 (254)	5.0 (0.4)	9.9
3	water pH 5	12.18 (0.31)	4199 (141)	272 (54)	4248 (153)	6.0 (0.5)	34.3
	water pH 10	12.67 (0.05)	4964 (146)	152 (34)	5361 (127)	2.3 (0.3)	22.2
	MTBE	13.68 (0.24)	5414 (124)	325 (45)	4797 (325)	7.0 (0.4)	15.3
	THF	13.30 (0.25)	5197 (103)	211 (59)	4914 (103)	7.0 (0.5)	18.7
4	water pH 5	11.63 (0.20)	3583 (158)	205 (15)	3803 (102)	10.1 (1.0)	33.9
	water pH 10	13.02 (0.15)	4370 (240)	136 (34)	4911 (128)	4.2 (0.4)	19.2
	MTBE	13.08 (0.18)	4954 (190)	335 (37)	4478 (130)	8.3 (0.6)	8.6
	THF	13.94 (0.24)	5282 (220)	471 (45)	4616 (134)	9.2 (0.5)	2.5
5	water pH 5	11.82 (0.18)	3759 (145)	220 (24)	3637 (114)	7.5 (0.4)	34.1
	water pH 10	14.00 (0.31)	5058 (189)	130 (16)	5566 (254)	4.4 (0.2)	14.7
	MTBE	14.01 (0.30)	5162 (176)	320 (31)	5419 (312)	5.2 (0.4)	9.6
	THF	14.11 (0.29)	5661 (210)	423 (37)	5353 (285)	6.3 (0.6)	4.3

<sup>&</sup>lt;sup>a</sup>These values are provided for five different models in three solvents and at two pH values in water. Standard deviations shown in parentheses. <sup>b</sup>Calculated as the ratio of SASA of model after equilibration to the initial one. Initial SASA is a sum of SASA of individual DOM molecules in the model.

observed for other  $\pi$ -stacking aggregates. This result verifies that, even if  $\pi$ -stacked clusters were present in water, they would spontaneously dissociate in MTBE, THF, or in other low-polarity solvents.

**Implications for Optical Properties.** Based on the results from this work, the configuration between aromatic rings that enables CT excitation to occur is primarily  $\pi$ -stacking, which forms very close intermolecular interactions. The closer the molecules are, the greater the extent of charge-transfer excitation due to increased overlap of the HOMO and the LUMO of the donor and acceptor, respectively.<sup>68</sup> Because of closer interactions of dipoles, new energy levels were created, the effect of which will be observed in the absorbance and fluorescence spectra of molecules. To verify the impact of the formation of  $\pi$ -stacking clusters on the absorbance spectra, we calculated the absorption spectra for esculetin and syringaldehyde and their  $\pi$ -stacking cluster in water (no calculations were made in other solvents given that these clusters are not expected to form). The calculation of absorption spectra for individual molecules and formed a  $\pi$ -stacking cluster shows the increase in the absorption maximum wavelength (see Figure 4). The  $\pi$ -stacking cluster resulted in an additional absorption

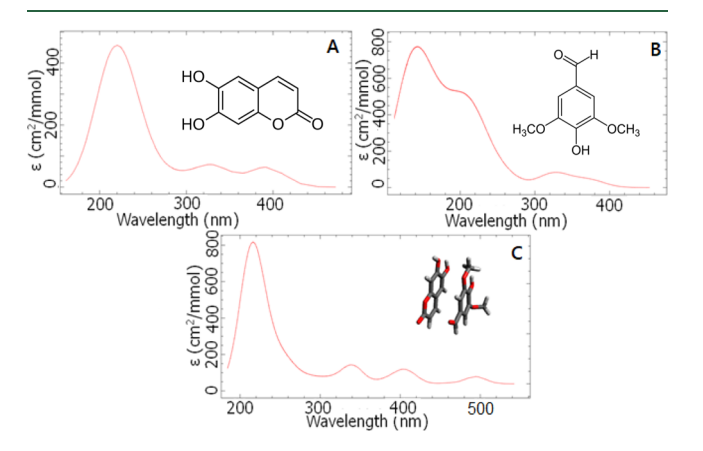


**Figure 4.** UV spectra for esculetin (A) and syringaldehyde (B) as well as spectrum for the  $\pi$ -stacked aggregate (C) formed by both compounds. The  $\pi$ -stacked aggregate results in a new accessible absorbance band with a wavelength maximum of 494 nm. The spectra calculated with the TD-DFT and BP86 aug-cc-pVDZ setting.

band centered at around 494 nm, a transition that is not available for either of the individual components. The calculated charge-transfer value, <sup>69</sup> represented as q(CT), for the observed complex was between 0.95 and 1.00, which additionally confirmed the charge transfer between the donor and the acceptor (Figure S4, Supporting Information).

According to the CT model presented by Blough and Del Vecchio, chromophores involved in DA complexes should be partly solvent-inaccessible, as it is presented in Figure 5a. <sup>17,18,70</sup> This model is based, in part, on a work by Dreyer et al., <sup>71</sup> who postulated that noncovalent interactions (i.e., CT) are responsible for the primary structure of polydopamine. Polydopamine contains 1,2-dihydroxyindole and its corresponding dione, <sup>71</sup> which Blough and Del Vecchio argued are structurally related to potential donor—acceptor moieties within DOM. <sup>17,70</sup>

To test the solvent accessibility of DOM chromophores, we examined the changes in SASA upon model equilibration and also examined the solvent accessibility of O and C atoms in our equilibrated models. A comparison of initial SASA (calculated as a sum of SASA for individual molecules) and after REMD simulations indicates a drop of 21 to 34% after systems reached an equilibrium in water solvent at pH 5, indicating the presence of some HbSA (Table 1). Although, at lower concentrations (model #1 3000 water molecules), the drop in SASA was lower, 5.5%. Further calculation of the number of surface and buried atoms (atoms inaccessible to the 1.4 Å water probe) (GETAREA<sup>72</sup>) for models at pH 5 in water solvent showed that the number of solvent-inaccessible oxygen atoms was 2-5 out of 98-110 oxygen atoms (or 0.02-0.05%) of organic matter in the system, and the number of buried carbon atoms varied between 9 (model 3, pH 5) to 36 (model 6, pH 5) out of 173-196 total carbon atoms (10.0-19.4%) in SFRA models (Table S4, Supporting Information). Similarly, for the model with lower DOM concentrations ( $\sim$ 7%), the size of hydrophobic "pockets" decreased, resulting in 7.5% of C atoms being solvent inaccessible. Therefore, we can conclude that a majority of oxygen-containing functional groups were solvent accessible, and the observed decrease in SASA occurred due to migration of hydrophobic carbon and hydrogen atoms to the centers of the aggregate's 3D

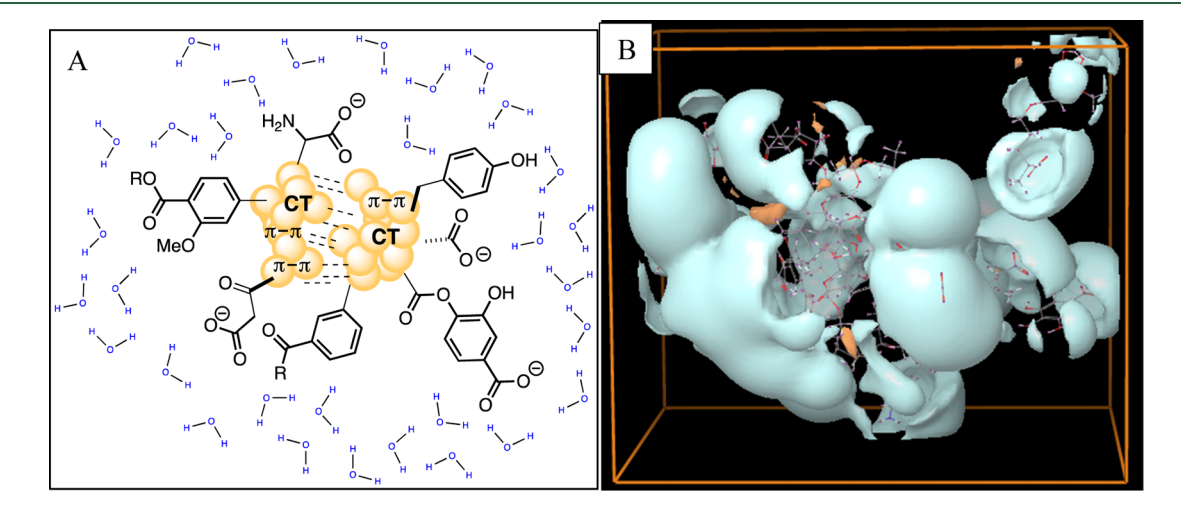


Figure 5. (A) Model of solvent inaccessible CT contacts within DOM. (B) Hydrophilic (blue) and hydrophobic (orange) surface areas calculated for model #1, pH 5.

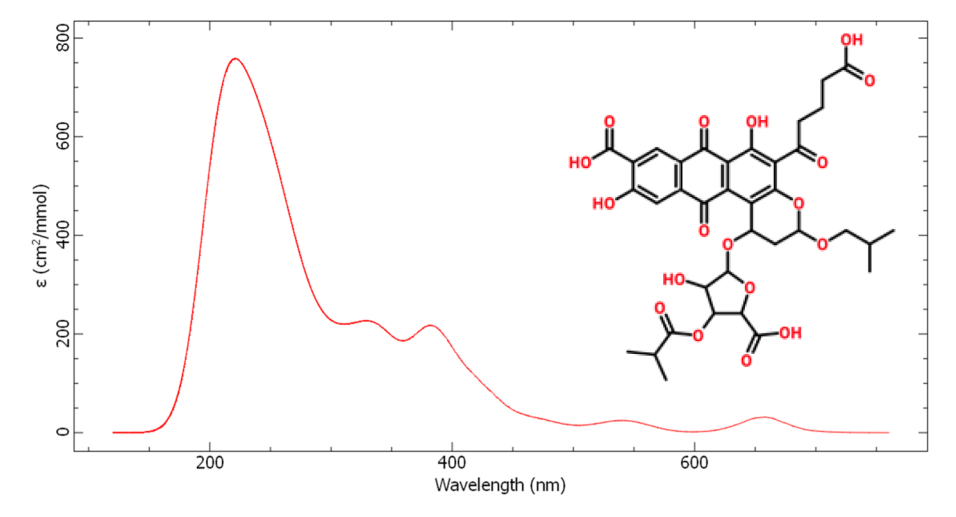


Figure 6. Calculated UV-spectra for a SRFA component in water with the sTD-DFT BP86 aug-cc-pVDZ setting.

configurations. Conversely, the majority of oxygen-containing functional groups remain solvent accessible (Figure 5b).

One of the key arguments in the CT model for optical properties of DOM is how to explain the longer wavelength absorption (wavelengths longer than ~350 nm).<sup>73</sup> It is assumed that given the lack of known chromophores that absorb in this region, CT excitation could be responsible. Figure 4 presents computational evidence for the role of electronically interacting chromophores contributing to longer wavelength absorption within SRFA. However, using the same computational methods, we can also calculate the absorption spectra for other potential components of DOM. Figure 6 presents the absorbance spectra for a molecule used in models #1 and #4. In this case, it is clearly observed how this molecule has absorbance bands beyond 350 nm. Therefore, it is expected that components such as coumarins and flavin/ flavonoid<sup>74</sup> derivatives<sup>75,76</sup> can contribute to the absorbance of DOM, even if they represent a very low fraction of the total carbon.13

Implications for the Study of DOM Photophysics. The work presented herein can be used to further our collective understanding of the underlying photophysical model of the optical properties of DOM. The study of these properties, visà-vis, the study of DOM photophysics, represents an area of research where we lack clarity. An important contribution was presented in 2004, with the publication of the work by Del Vecchio and Blough, 12 which suggested that a significant portion of the observable optical properties was due to the existence of CT complexes. As described (vide supra), these complexes are expected to be formed between electron donors (e.g., phenolic structures) and electron acceptors (e.g., quinones, aromatic ketones/aldehydes), and result in the formation of new optical transitions, accessible at longer wavelengths beyond the maximum absorbance peak for the individual components. In a recent publication, a challenge to this model was presented via the lack of impact of solvent polarity and temperature on the observed optical properties of DOM isolates. 16 This challenge was based on the idea that potential DA complexes are expected to be solvent accessible. A counter argument was presented in which it is hypothesized that the DA complexes are mostly solvent inaccessible. <sup>17</sup> The proposed solvent inaccessibility of the DA complexes would thus explain both their importance regarding the observable optical properties of DOM and also the lack of effect of solvent

polarity and temperature. It is worth mentioning that these inaccessible DA complexes would then be hydrophobic in nature and also very strong both in terms of thermodynamics and kinetic stability.

The work presented herein, although computational in nature, provides important considerations for the larger study of DOM photophysics. First, we show that the presence of large hydrophobic centers in carefully constructed models of DOM (based on common chromophores and FTICR-MS data) is, in general, limited. Simulations revealed that most of the oxygen-containing functional groups, including phenolic and quinoid moieties, are solvent accessible in water, as could be expected from their hydrophilic nature. Second, based on aqueous solubility estimations, most chromophores (and fluorophores) are expected to be solvent accessible, rather than in a hydrophobic environment. This is also consistent with the observed photochemical behavior of the same groups, in which polar probe molecules are able to measure the reactivity of these groups. Third, calculations of UV spectra for some chromophores with extensive conjugation systems (and for which chemical standards are not available), such as coumarins, flavins/flavonoids, and their derivatives, 74 show that the absorbance bands can extend into the visible region.

Our computational assessment of the three-dimensional configuration of DOM provides an insight into earlier experimental studies that have shown evidence for an aggregated three-dimensional DOM structure. Data in Table 1 and Figure S4 (Supporting Information) clearly demonstrate the formation of hydrophobic pockets, for example, decrease of SASA by 20-34% and presence of 5.2-19.4% of buried carbon atoms for organic models in water solvent at pH 5. Prior computational work by Vialykh et al.<sup>38</sup> demonstrated that hydrophobic probe molecules (like benzene) were readily able to partition into such pockets, whereas hydrophilic probe molecules (e.g., phenol) were not able to do so. This partitioning may explain more broadly the sorption of organic contaminants on DOM and their associated photochemical reactivity. For example, work by Latch and McNeill<sup>22</sup> demonstrated enhanced singlet-oxygen steady-state concentrations in the DOM microheterogeneous environment based on sensitization of a hydrophobic singlet oxygen probe relative to furfuryl alcohol (an aqueous phase probe). Follow-up studies by Grandbois et al.<sup>77</sup> acknowledged that DOM molecular weights calculated from the Latch and McNeill

model were erroneously large. Therefore, instead of hydrophobic singlet oxygen probes sorbing onto a DOM micelle, our results suggest that sorption of such probes may occur in hydrophobic pockets with DOM in more of an aggregated three-dimensional structure, and thereby be exposed to enhanced singlet oxygen concentrations. These enhanced singlet oxygen concentrations may be due, in part, to both decreased quenching of singlet oxygen by water molecules in these hydrophobic pockets, as previously argued by Latch and McNeill, or to the closer proximity of the hydrophobic probes and singlet oxygen sensitizers (which may potentially reside in the hydrophobic pocket themselves).

The incomplete reduction of DOM by sodium borohydride has also been taken as evidence of DOM's aggregated threedimensional structure. 18,25,78 The rationale here is that borohydride (BH<sub>4</sub><sup>-</sup>), an anion, is unable to access all CT contacts due to repulsion by DOM carboxylate groups. While our computational results indeed show evidence of such CT behavior, it is unclear if this can completely explain the lack of complete borohydride reduction of DOM in water solvent models.

Another conclusion from this work relates to the expectation of CT bands to be present in the DOM absorbance spectra. As shown in Figures 4 and S4,  $\pi$ -stacking interactions are observed in our SRFA models, with subsequent effects on the calculated absorbance spectra. These results offer computational confirmation of CT interactions within DOM and impacts on optical properties.

Although this computational work only focused on CDOM, it is expected that the results will also inform the study of fluorophoric DOM. Several fluorophores were included in the above models, and as in the case of chromophores, these fluorophores were mostly water accessible. However, much remains to be assessed regarding the optical properties of DOM, including the now well-documented observation of lowfluorescence quantum yields and wavelength dependence for these values.

In context of the ongoing discussion regarding the prevalence of the CT model to explain the optical properties of DOM,  $^{16,17,79}$  it was shown that formation of  $\pi$ -stacking clusters occurred in water solvent, and replacement of the solvent with nonpolar ones results in disruption of  $\pi$ -stacking structures as well as the whole molecular assemblies. This result further highlights the dynamic nature of these assemblies. The solvophobic interactions of the relatively nonpolar aromatic units in a strongly interacting polar solvent, that is, the hydrophobic effect, and its effect on association constant in different solvents were shown by Ikkanda. 80 The findings of Ikkanda are in agreement with our results, which showed the absence of  $\pi$ -stacking assemblies in THB and MTBE solvents. Consequently, the formation of CT complexes via  $\pi$ -stacking clusters in nonpolar solvents is insignificant and cannot contribute to the absorption max of UV spectra significantly as the optical properties of DOM did not change in different solvents. 16

Finally, this work also provides additional computational evidence of the potential of DOM to form aggregated threedimensional structures in water, albeit in a somewhat limited scale. This work can also help understand other known processes within DOM, including the partitioning of hydrophobic organic compounds.

### ASSOCIATED CONTENT

# Supporting Information

The Supporting Information is available free of charge at https://pubs.acs.org/doi/10.1021/acs.est.0c05860.

An example of log D solubility calculation for a molecule; molecular composition of the different models created and calculated values for log D and maximum absorbance; description of the ReaxFF force field; time series of replicas at 300 K for REMD simulations of model #1 in water solvent at pH 5; probability distribution of potential energy at the first seven and at the last five temperatures; charge-transfer complex formed in model 3 pH 5 water solvent and calculated excited-state characteristics; percentage of buried carbon and oxygen atoms of organic molecules in different solvents; and a model in water and THF (PDF)

# AUTHOR INFORMATION

# **Corresponding Author**

Fernando L. Rosario-Ortiz - Department of Civil, Environmental, and Architectural Engineering and Environmental Engineering Program, University of Colorado Boulder, Boulder, Colorado 80309, United States;

orcid.org/0000-0002-3311-9089; Email: Fernando.rosario@colorado.edu

#### **Authors**

Elena A. Vialykh - Department of Civil, Environmental, and Architectural Engineering, University of Colorado Boulder, Boulder, Colorado 80309, United States

Garrett McKay - Zachry Department of Civil & Environmental Engineering, Texas A&M University, College Station, Texas 77843, United States; o orcid.org/0000-

Complete contact information is available at: https://pubs.acs.org/10.1021/acs.est.0c05860

The authors declare no competing financial interest.

### ACKNOWLEDGMENTS

Partial funding for this study came from the US National Science Foundation (CBET #1453906). This work utilized resources from the University of Colorado Boulder Research Computing Group, which was supported by the National Science Foundation (awards ACI-1532235 and ACI-1532236), the University of Colorado Boulder, and Colorado State University.

# REFERENCES

- (1) Coble, P. G. Characterization of Marine and Terrestrial DOM in Seawater Using Excitation-Emission Matrix Spectroscopy. Mar. Chem. 1996, 51, 325-346.
- (2) Coble, P. G. Marine Optical Biogeochemistry: The Chemistry of Ocean Color. Chem. Rev. 2007, 107, 402-418.
- (3) Shapiro, J. Chemical and Biological Studies on the Yellow Organic Acids of Lake Water1. Limnol. Oceanogr. 1957, 2, 161-179.
- (4) Green, S. A.; Blough, N. V. Optical Absorption and Fluorescence Properties of Chromophoric Dissolved Organic Matter in Natural Waters. Limnol. Oceanogr. 1994, 39, 1903-1916.
- (5) Vaughan, M. C. H.; Bowden, W. B.; Shanley, J. B.; Vermilyea, A.; Schroth, A. W. Shining Light on the Storm: In-Stream Optics Reveal

- Hysteresis of Dissolved Organic Matter Character. *Biogeochemistry* **2019**, *143*, 275–291.
- (6) Chen, Y.; Arnold, W. A.; Griffin, C. G.; Olmanson, L. G.; Brezonik, P. L.; Hozalski, R. M. Assessment of the Chlorine Demand and Disinfection Byproduct Formation Potential of Surface Waters via Satellite Remote Sensing. *Water Res.* **2019**, *165*, 115001.
- (7) Korak, J. A.; Rosario-Ortiz, F. L.; Summers, R. S. Evaluation of Optical Surrogates for the Characterization of DOM Removal by Coagulation. *Environ. Sci.: Water Res. Technol.* **2015**, *1*, 493–506.
- (8) Ulliman, S. L.; Korak, J. A.; Linden, K. G.; Rosario-Ortiz, F. L. Methodology for Selection of Optical Parameters as Wastewater Effluent Organic Matter Surrogates. *Water Res.* **2020**, *170*, 115321.
- (9) Cory, R. M.; Ward, C. P.; Crump, B. C.; Kling, G. W. Sunlight Controls Water Column Processing of Carbon in Arctic Fresh Waters. *Science* **2014**, 345, 925–928.
- (10) Mckay, G.; Huang, W.; Romera-Castillo, C.; Crouch, J. E.; Rosario-Ortiz, F. L.; Jaffé, R. Predicting Reactive Intermediate Quantum Yields from Dissolved Organic Matter Photolysis Using Optical Properties and Antioxidant Capacity. *Environ. Sci. Technol.* **2017**, *51*, 5404–5413.
- (11) Peterson, B. M.; McNally, A. M.; Cory, R. M.; Thoemke, J. D.; Cotner, J. B.; McNeill, K. Spatial and Temporal Distribution of Singlet Oxygen in Lake Superior. *Environ. Sci. Technol.* **2012**, *46*, 7222–7229.
- (12) Del Vecchio, R.; Blough, N. V. On the Origin of the Optical Properties of Humic Substances. *Environ. Sci. Technol.* **2004**, 38, 3885–3891.
- (13) McKay, G. Emerging Investigator Series: Critical Review of Photophysical Models for the Optical and Photochemical Properties of Dissolved Organic Matter. *Environ. Sci.: Processes Impacts* **2020**, 22, 1139–1165.
- (14) Peuravuori, J.; Pihlaja, K. Molecular Size Distribution and Spectroscopic Properties of Aquatic Humic Substances. *Anal. Chim. Acta* **1997**, 337, 133–149.
- (15) Twardowski, M. S.; Boss, E.; Sullivan, J. M.; Donaghay, P. L. Modeling the Spectral Shape of Absorption by Chromophoric Dissolved Organic Matter. *Mar. Chem.* **2004**, *89*, 69–88.
- (16) McKay, G.; Korak, J. A.; Erickson, P. R.; Latch, D. E.; McNeill, K.; Rosario-Ortiz, F. L. The Case Against Charge Transfer Interactions in Dissolved Organic Matter Photophysics. *Environ. Sci. Technol.* **2018**, 52, 406–414.
- (17) Blough, N. V.; Del Vecchio, R. Comment on The Case Against Charge Transfer Interactions in Dissolved Organic Matter Photophysics. *Environ. Sci. Technol.* **2018**, *52*, 5512–5513.
- (18) Schendorf, T. M.; Del Vecchio, R.; Bianca, M.; Blough, N. V. Combined Effects of PH and Borohydride Reduction on Optical Properties of Humic Substances (HS): A Comparison of Optical Models. *Environ. Sci. Technol.* **2019**, *53*, 6310–6319.
- (19) Sharpless, C. M.; Blough, N. V. The Importance of Charge-Transfer Interactions in Determining Chromophoric Dissolved Organic Matter (CDOM) Optical and Photochemical Properties. *Environ. Sci.: Processes Impacts* **2014**, *16*, 654–671.
- (20) Dalrymple, R. M.; Carfagno, A. K.; Sharpless, C. M. Correlations between Dissolved Organic Matter Optical Properties and Quantum Yields of Singlet Oxygen and Hydrogen Peroxide. *Environ. Sci. Technol.* **2010**, *44*, 5824–5829.
- (21) Sharpless, C. M. Lifetimes of Triplet Dissolved Natural Organic Matter (DOM) and the Effect of NaBH4 Reduction on Singlet Oxygen Quantum Yields: Implications for DOM Photophysics. *Environ. Sci. Technol.* **2012**, *46*, 4466–4473.
- (22) Latch, D. E.; McNeill, K. Microheterogeneity of Singlet Oxygen Distributions in Irradiated Humic Acid Solutions. *Science* **2006**, *311*, 1743–1747.
- (23) Aeschbacher, M.; Sander, M.; Schwarzenbach, R. P. Novel Electrochemical Approach to Assess the Redox Properties of Humic Substances. *Environ. Sci. Technol.* **2010**, *44*, 87–93.
- (24) Canonica, S.; Jans, U.; Stemmler, K.; Hoigne, J. Transformation Kinetics of Phenols in Water: Photosensitization by Dissolved Natural

- Organic Material and Aromatic Ketones. Environ. Sci. Technol. 1995, 29, 1822-1831.
- (25) Ma, J.; Del Vecchio, R.; Golanoski, K. S.; Boyle, E. S.; Blough, N. V. Optical Properties of Humic Substances and CDOM: Effects of Borohydride Reduction. *Environ. Sci. Technol.* **2010**, *44*, 5395–5402.
- (26) Ossola, R.; Tolu, J.; Clerc, B.; Erickson, P. R.; Winkel, L. H. E.; McNeill, K. Photochemical Production of Sulfate and Methanesulfonic Acid from Dissolved Organic Sulfur. *Environ. Sci. Technol.* **2019**, 53, 13191–13200.
- (27) Önnby, L.; Salhi, E.; McKay, G.; Rosario-Ortiz, F. L.; von Gunten, U. Ozone and Chlorine Reactions with Dissolved Organic Matter Assessment of Oxidant-Reactive Moieties by Optical Measurements and the Electron Donating Capacities. *Water Res.* **2018**, *144*, 64–75.
- (28) Maizel, A. C.; Remucal, C. K. Molecular Composition and Photochemical Reactivity of Size-Fractionated Dissolved Organic Matter. *Environ. Sci. Technol.* **2017**, *51*, 2113–2123.
- (29) McKay, G.; Couch, K. D.; Mezyk, S. P.; Rosario-Ortiz, F. L. Investigation of the Coupled Effects of Molecular Weight and Charge-Transfer Interactions on the Optical and Photochemical Properties of Dissolved Organic Matter. *Environ. Sci. Technol.* **2016**, *50*, 8093–8102
- (30) Sutton, R.; Sposito, G.; Diallo, M. S.; Schulten, H.-R. Molecular Simulation of a Model of Dissolved Organic Matter. *Environ. Toxicol. Chem.* **2005**, *24*, 1902–1911.
- (31) Orsi, M. Molecular Dynamics Simulation of Humic Substances. *Chem. Biol. Technol. Agric.* **2014**, *1*, 10.
- (32) Petrov, D.; Tunega, D.; Gerzabek, M. H.; Oostenbrink, C. Molecular Dynamics Simulations of the Standard Leonardite Humic Acid: Microscopic Analysis of the Structure and Dynamics. *Environ. Sci. Technol.* **2017**, *51*, 5414–5424.
- (33) Feng, H.; Zhang, H.; Cao, H.; Sun, Y.; Zhang, A.; Fu, J. Application of a Novel Coarse-Grained Soil Organic Matter Model in the Environment. *Environ. Sci. Technol.* **2018**, *52*, 14228–14234.
- (34) Liang, Y.; Ding, Y.; Wang, P.; Lu, G.; Dang, Z.; Shi, Z. Molecular Characteristics, Proton Dissociation Properties, and Metal Binding Properties of Soil Organic Matter: A Theoretical Study. *Sci. Total Environ.* **2019**, *656*, 521–530.
- (35) Piccolo, A. The Supramolecular Structure of Humic Substances: A Novel Understanding of Humus Chemistry and Implications in Soil Science. *Adv. Agron.* **2002**, *75*, 57–134.
- (36) van Duin, A. C. T.; Dasgupta, S.; Lorant, F.; Goddard, W. A. ReaxFF: A Reactive Force Field for Hydrocarbons. *J. Phys. Chem. A* **2001**, *105*, 9396–9409.
- (37) Leenheer, J. A.; McKnight, D. M.; Thurman, E. M.; MacCarthy, P. Structural Components and Proposed Structural Models of Fulvic Acid from the Suwannee River. In *Humic Substances in the Suwannee River, Georgia: Interactions, Properties, and Proposed Structures*; Averett, R. C., Leenheer, J. A., McKnight, D. M., Thorn, K. A., Eds.; US Geological Servey, No 87-557; U.S. G.P.O.; U.S. Geological Survey, Map Distribution, 1994; pp 195–212.
- (38) Vialykh, E. A.; Salahub, D. R.; Achari, G.; Cook, R. L.; Langford, C. H. Emergent Functional Behaviour of Humic Substances Perceived as Complex Labile Aggregates of Small Organic Molecules and Oligomers. *Environ. Chem.* 2019, 16, 505.
- (39) Vialykh, E. A.; Salahub, D. R.; Achari, G. Metal Ion Binding by Humic Substances as Emergent Functions of Labile Supramolecular Assemblies. *Environ. Chem.* **2020**, *17*, 252–265.
- (40) Wünsch, U. J.; Murphy, K. R.; Stedmon, C. A. Fluorescence Quantum Yields of Natural Organic Matter and Organic Compounds: Implications for the Fluorescence-Based Interpretation of Organic Matter Composition. *Front. Mar. Sci.* **2015**, *2*, 98.
- (41) Remucal, C. K.; Cory, R. M.; Sander, M.; McNeill, K. Low Molecular Weight Components in an Aquatic Humic Substance As Characterized by Membrane Dialysis and Orbitrap Mass Spectrometry. *Environ. Sci. Technol.* **2012**, *46*, 9350–9359.
- (42) Green, N. W.; Perdue, E. M. Fast Graphically Inspired Algorithm for Assignment of Molecular Formulae in Ultrahigh Resolution Mass Spectrometry. *Anal. Chem.* **2015**, *87*, 5086–5094.

- (43) PubChem. PubChem. https://pubchem.ncbi.nlm.nih.gov/(accessed Jul 24, 2020).
- (44) Kalinichev, A. G.; Kirkpatrick, R. J. Molecular Dynamics Simulation of Cationic Complexation with Natural Organic Matter. *Eur. J. Soil Sci.* **2007**, *58*, 909–917.
- (45) ChemAxon—Software Solutions and Services for Chemistry & Biology. https://chemaxon.com/ (accessed Jul 27, 2020).
- (46) Aiken, G. R.; Malcolm, R. L. Molecular Weight of Aquatic Fulvic Acids by Vapor Pressure Osmometry. *Geochim. Cosmochim. Acta* 1987, 51, 2177–2184.
- (47) Martínez, L.; Andrade, R.; Birgin, E. G.; Martínez, J. M. PACKMOL: A Package for Building Initial Configurations for Molecular Dynamics Simulations. *J. Comput. Chem.* **2009**, *30*, 2157–2164.
- (48) Monti, S.; Corozzi, A.; Fristrup, P.; Joshi, K. L.; Shin, Y. K.; Oelschlaeger, P.; van Duin, A. C. T.; Barone, V. Exploring the Conformational and Reactive Dynamics of Biomolecules in Solution Using an Extended Version of the Glycine Reactive Force Field. *Phys. Chem. Chem. Phys.* **2013**, *15*, 15062–15077.
- (49) Zhang, W.; van Duin, A. C. T. Improvement of the ReaxFF Description for Functionalized Hydrocarbon/Water Weak Interactions in the Condensed Phase. *J. Phys. Chem. B* **2018**, *122*, 4083–4092.
- (50) LAMMPS. 1. Introduction—LAMMPS documentation https://lammps.sandia.gov/doc/Intro.html (accessed Oct 14, 2020).
- (51) Rhodes, G. Chapter 9-Other Diffraction Methods. In Crystallography Made Crystal Clear 3rd ed.; Rhodes, G., Ed.; Complementary Science; Academic Press: Burlington, 2006; pp 211–235.
- (52) Humphrey, W.; Dalke, A.; Schulten, K. VMD: Visual Molecular Dynamics. *J. Mol. Graphics* **1996**, *14*, 33–38.
- (53) UCSF Chimera Home Page. http://www.rbvi.ucsf.edu/chimera/ (accessed Oct 14, 2020).
- (54) Maestro 11; Schrödinger. https://www.schrodinger.com/maestro (accessed Dec 11, 2017).
- (55) Neese, F. The ORCA Program System. Wiley Interdiscip. Rev.: Comput. Mol. Sci. 2012, 2, 73–78.
- (56) Plasser, F.; Wormit, M.; Dreuw, A. New Tools for the Systematic Analysis and Visualization of Electronic Excitations. I. Formalism. *J. Chem. Phys.* **2014**, *141*, 024106.
- (57) TheoDORE. http://theodore-qc.sourceforge.net/ (accessed Jul 24, 2020).
- (58) Sugita, Y.; Okamoto, Y. Replica-Exchange Multicanonical Algorithm and Multicanonical Replica-Exchange Method for Simulating Systems with Rough Energy Landscape. *Chem. Phys. Lett.* **2000**, 329, 261–270.
- (59) Periole, X.; Mark, A. E. Convergence and Sampling Efficiency in Replica Exchange Simulations of Peptide Folding in Explicit Solvent. *J. Chem. Phys.* **2007**, *126*, 014903.
- (60) Cheng, X.; Cui, G.; Hornak, V.; Simmerling, C. Modified Replica Exchange Simulation Methods for Local Structure Refinement. *J. Phys. Chem. B* **2005**, *109*, 8220–8230.
- (61) Yang, Y.; Pan, L.; Lightstone, F. C.; Merz, K. M. The Role of Molecular Dynamics Potential of Mean Force Calculations in the Investigation of Enzyme Catalysis. *Methods Enzymol.* **2016**, *577*, 1–29.
- (62) Grossfield, A. An Implementation of WHAM: The Weighted Histogram Analysis Method, version 2.0.9. 18.
- (63) Gallicchio, E.; Andrec, M.; Felts, A. K.; Levy, R. M. Temperature Weighted Histogram Analysis Method, Replica Exchange, and Transition Paths. *J. Phys. Chem. B* **2005**, *109*, 6722–6731.
- (64) Chodera, J. D.; Swope, W. C.; Pitera, J. W.; Seok, C.; Dill, K. A. Use of the Weighted Histogram Analysis Method for the Analysis of Simulated and Parallel Tempering Simulations. *J. Chem. Theory Comput.* **2007**, *3*, 26–41.
- (65) Bruccoleri, A. G.; Sorenson, B. T.; Langford, C. H. Molecular Modelling of Humic Structures. In *Humic Substances: Structures*,

- Models and Functions; Ghabbour, E. A., Davies, G., Eds.; Royal Society of Chemistry: Great Britain, 2001; pp 193–208.
- (66) Schulten, H.-R.; Thomsen, M.; Carlsen, L. Humic Complexes of Diethyl Phthalate: Molecular Modelling of the Sorption Process. *Chemosphere* **2001**, *45*, 357–369.
- (67) Schulten, H.-R.; Leinweber, P. New Insights into Organic-Mineral Particles: Composition, Properties and Models of Molecular Structure. *Biol. Fertil. Soils* **2000**, *30*, 399–432.
- (68) Tossell, J. A. Quinone-Hydroquinone Complexes as Model Components of Humic Acids: Theoretical Studies of Their Structure, Stability and Visible-UV Spectra. *Geochim. Cosmochim. Acta* **2009**, 73, 2023–2033.
- (69) Plasser, F.; Lischka, H. Analysis of Excitonic and Charge Transfer Interactions from Quantum Chemical Calculations. *J. Chem. Theory Comput.* **2012**, *8*, 2777–2789.
- (70) Del Vecchio, R.; Schendorf, T. M.; Blough, N. V. Contribution of Quinones and Ketones/Aldehydes to the Optical Properties of Humic Substances (HS) and Chromophoric Dissolved Organic Matter (CDOM). *Environ. Sci. Technol.* **2017**, *51*, 13624–13632.
- (71) Dreyer, D. R.; Miller, D. J.; Freeman, B. D.; Paul, D. R.; Bielawski, C. W. Elucidating the Structure of Poly(Dopamine). *Langmuir* **2012**, *28*, 6428–6435.
- (72) GetArea. http://curie.utmb.edu/getarea.html (accessed Jul 27, 2020).
- (73) Boyle, E. S.; Guerriero, N.; Thiallet, A.; Vecchio, R. D.; Blough, N. V. Optical Properties of Humic Substances and CDOM: Relation to Structure. *Environ. Sci. Technol.* **2009**, *43*, 2262–2268.
- (74) Grimm, J. B.; Heckman, L. M.; Lavis, L. D. The Chemistry of Small-Molecule Fluorogenic Probes. In *Progress in Molecular Biology and Translational Science*; Elsevier, 2013; Vol. 113, pp 1–34. DOI: DOI: 10.1016/B978-0-12-386932-6.00001-6.
- (75) Momzikoff, A. Study of the Fluorescent Components of the Sea-Water. Identification of Isoxanthopterin, Riboflavine and Lumichrome. *Cah. Biol. Mar.* **1969**, *10*, 221–230.
- (76) Gaill, F.; Momzikoff, A. The Presence of Riboflavin and Two Pterins in Ascidians (Tunicata) and Their Excretion into Sea Water. *Mar. Biol.* **1975**, *29*, 315–319.
- (77) Grandbois, M.; Latch, D. E.; McNeill, K. Microheterogeneous Concentrations of Singlet Oxygen in Natural Organic Matter Isolate Solutions. *Environ. Sci. Technol.* **2008**, *42*, 9184–9190.
- (78) Schendorf, T. M.; Del Vecchio, R.; Koech, K.; Blough, N. V. A Standard Protocol for NaBH4 Reduction of CDOM and HS. *Limnol. Oceanogr.: Methods* **2016**, *14*, 414–423.
- (79) McKay, G.; Korak, J. A.; Erickson, P. R.; Latch, D. E.; McNeill, K.; Rosario-Ortiz, F. L. Response to Comment on The Case Against Charge Transfer Interactions in Dissolved Organic Matter Photophysics. *Environ. Sci. Technol.* **2018**, *52*, 5514–5516.
- (80) Ikkanda, B. A.; Iverson, B. L. Exploiting the Interactions of Aromatic Units for Folding and Assembly in Aqueous Environments. *Chem. Commun.* **2016**, *52*, 7752–7759.